

The Generalized SEA to UXO Discrimination in Geophysical Environments Producing EMI Response

F. Shubitidze⁽¹⁾, B. E. Barrowes⁽²⁾, K. O'Neill^(1,2), I. Shamatava⁽¹⁾,
J. P. Fernández⁽¹⁾, K. Sun⁽¹⁾, and K.D. Paulsen⁽¹⁾

⁽¹⁾ Thayer School of Engineering, Dartmouth College, Hanover, NH 03755, USA

Email: Fridon.Shubitidze@dartmouth.edu

⁽²⁾ USA ERDC Cold Regions Research and Engineering Laboratory,
72 Lyme Road, Hanover, NH 03755, USA

Abstract - The generalized standardized excitation approach (GSEA) is presented to enhance UXO discrimination under realistic field conditions. The GSEA is a fast, numerical, forward model for representing an object's EMI responses over the entire frequency band from near DC to 100s of kHz. It has been developed and tested in both the frequency and time domains for actual UXOs placed in free space. The GSEA, which uses magnetic dipoles instead of magnetic charges as responding sources, is capable of taking into account the background medium surrounding an object. Given a modeled UWB frequency domain (FD) response, the corresponding time domain (TD) response is easily obtained by the inverse Fourier transform. Thus the technique is applicable for any FD or TD sensor configuration and can treat complex data sets: novel waveforms, multi-axis, vector, or tensor magnetic or electromagnetic induction data, or any combination of magnetic and EMI data. Host media effects are taken into account via appropriate types of Green's function and equivalent dipole sources. Comparisons between simulations and experimental data illustrate that the GSEA is a unified approach for reproducing both TD and FD EMI signals for actual UXOs. The EMI response from a soil that has a frequency-dependent magnetic susceptibility is studied. The EMI responses in both FD and TD domains are analyzed for the model of an actual UXO that is buried in a magnetically susceptible half space.

Keywords: dipole, discrimination, Green's function, magnetic soil, modeling, UXO.

1. INTRODUCTION

Cleanup of unexploded ordnance (UXO) from former military ranges and battlefields continues to be a most pressing military environmental problem worldwide. A wide range of different sensing technologies is being used or is in development for detecting and discriminating UXOs. Among these technologies, metal detectors have been identified as one of most promising technologies for detection as well as classification of subsurface metallic objects. There are two types of metal detectors. One, that is called magnetometers, detects anomalies in the earth's magnetic field caused by ferrous (iron-based) objects [1]. The other, known as electromagnetic induction sensing, transmits an electromagnetic field that can lead to the detection of both ferrous and non-ferrous metals [2, 3]. Since these sensors can sense UXOs, they can detect everything else metallic in close proximity. Therefore, current discrimination techniques have great difficulties in distinguishing UXO from non-UXO metallic debris, found at most UXO sites.

The problem becomes much more complicated when signals are contaminated by noise that originates from magnetically susceptible and electrically conductive soils [4–16]. Until now, in most existing approaches to UXO classification, the object of interest is assumed to be placed in a free space [1, 17–26]. Any influence of the host medium is considered to be removed by filtering before data are submitted to an inversion algorithm. Recent studies show that “geologically hostile” sites cause significant problems for magnetometers and electromagnetic induction (EMI) sensors, in terms of both decreased probability of detection and increased probability of false alarm. In regions of highly magnetic soil, magnetometry and electromagnetic sensors often detect large anomalies that are of geologic, rather than of metallic, origin. For instance, [4] documented the problems encountered at the former Naval Training Range on Kaho’olawe Island when using EMI sensors. During production surveys at the site, approximately 30% of identified anomalies were from false positives due to geology, attributed to the strong magnetic viscosity exhibited by the basaltic soils.

There is also a need for detection and discrimination of UXO in undersea environments [27]. In this case, unlike land surveys where the conductivity ($<10^{-2}$ [S/m]) of non-permeable soils can be neglected, it is impossible to neglect EMI responses due to the conductivity of seawater and the ocean bottom in marine surveys. All of this leads to a high

level of false alarms, which translates into an increased workload because each detected anomaly must be treated as if it were an actual UXO. Therefore, innovative discrimination techniques that apply to any field condition and that reliably, quickly, and accurately distinguish between hazardous UXO and non-hazardous metallic items are required. To address this issue here we present a generalized standardized excitation approach (GSEA) that is suitable for complex data sets: novel waveforms, multi-axis, vector, tensor magnetic or electromagnetic induction data, or any combination of magnetic and EMI data.

The SEA for objects placed in free space is described in great detail in [24–26]. This work extends the SEA for more general cases by using magnetic dipoles as responding sources instead of magnetic charges as in [24–26]. By using magnetic dipoles with the corresponding dyadic Green’s function the GSEA becomes applicable for objects placed in a conducting and permeable host medium as well as in free space.

The GSEA can be briefly outlined as follows. For any given object the amplitudes of the responding magnetic dipoles are determined and sorted in the universal library for any number of basic spheroidal modes. Then, any primary field is decomposed into a set of basis excitations, which are then multiplied by appropriate weights (e.g., spheroidal modal decomposition coefficients from which we can calculate the target’s complete response just by superposing responses of each basic excitation). The key element in the GSEA is to determine the amplitudes of the responding sources, which are characteristic only of the object, and are independent of sensor type, object location and orientation, and transmitted waveforms.

There are two ways to determine the amplitudes on the responding magnetic dipoles: (1) using measurement data and (2) solving the full 3-D EMI problem in detail. The most straightforward way to determine the amplitudes of the responding magnetic dipole sources is to solve a standard inverse problem based on the measured data. Obviously, this process requires very good experimental conditions and a sufficient number of independent measurements of an object of interest in order to reduce the degree of ill-posedness. The ill-posedness makes the solution inaccurate. Recently, [26] applied such a data-derived approach to extracting the modal response coefficients for each candidate by carefully designing the measurements at different distances and orientations in free space. However, the accuracy and reliability of the model parameters determined in this way may not always be satisfactory due to unavoidable measurement noise and numerical difficulties arising from the inherent ill-conditioning of the problem, although a special treatment was applied in [26]. In addition, the model parameters were obtained from measurement data with the given sensor. Currently all available EMI sensors have certain limitations in both frequency band and time. Therefore, the amplitudes of the responding source that are derived from these measured data have limitations, they can’t cover all possible EMI and magnetic data, and they could not be used to obtain EMI response in time domain for different wave forms and sensors.

Originally, in [24] and [25], to determine the amplitudes of responding sources, a numerical procedure based on the method auxiliary source (MAS) and hybrid MAS thin skin approximation (MAS/TSA) was proposed and it is generalized here. In this procedure, by utilizing a full 3-D EMI solver, the modal responding coefficients, or strengths of a reduced source set (RSS) [24–25] are determined by employing a physically complete numerical simulation of the object’s response to each fundamental excitation mode. The full MAS model-based approach has an advantage over the data-derived-based approach, because it is a well-posed EMI problem and it is not dependent on measurements. In this approach the RSS can be obtained very accurately for any excitation mode and in an ultra-wide band frequency range. Thus, the technique allows users to calculate the EM field in both the frequency and time domain and to control the number of input spheroidal modes. Here the TD EMI response for a given UXO is calculated directly from FD RSS sources just by using the convolution theorem [28–30].

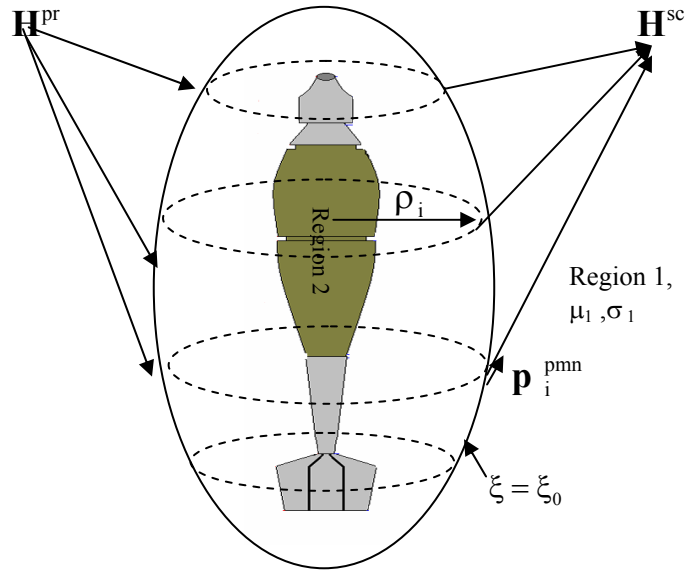


Figure 1. Problem geometry and reduced set of sources $\mathbf{p}_i^{\text{pmm}}$ distributed along rings on the spheroid surface.

The paper is organized as follows: In Section II, the generalized standardized excitation approach is presented, Section III describes the frequency-dependent magnetic susceptibility model, and Section IV shows several experimental and numerical results, demonstrating the applicability of the GSEA in both frequency and time domain, and for frequency-dependent magnetic soil.

2. GENERALIZED STANDARDIZED EXCITATION APPROACH

Recently, the SEA has been developed and applied to UXO discrimination [24–26]. All those studies assume that an object is placed in free space. Here, the SEA is generalized to take into account conducting and magnetically susceptible host media effects. To illustrate the GSEA, let us assume that an object is placed in a background with magnetic permeability μ_1 and conductivity σ_1 , Figure 1. The object is illuminated by an arbitrarily oriented, time-varying primary magnetic field. We surround the object with a fictitious spheroid, which is introduced only as a computational aide in the decomposition of the primary magnetic field into fundamental spheroidal modes. We choose spheroids because they can assume the general proportions of elongated objects of interest, such as UXO, which are also typically bodies of revolution (BOR). Oblate spheroids can also be used for flattened shapes. In general, the fictitious surface could be a smooth closed surface, as applicable for a related standardized source set approximation described in [24–25]. On the fictitious spheroid given by $\xi = \xi_0$ (Figure 1), the primary magnetic field can be expressed as:

$$\mathbf{H}^{\text{pr}} = \sum_{m=0}^{\infty} \sum_{n=m}^{\infty} \sum_{p=0}^1 b_{\text{pmn}} \mathbf{H}_{\text{pmn}}^{\text{pr}}. \quad (1)$$

The b_{pmn} are coefficients needed to express the primary field and $\mathbf{H}_{\text{pmn}}^{\text{pr}}$ is the pmn mode of the primary magnetic field component when $b_{\text{pmn}}=1$. The normal component of the primary magnetic field on the fictitious spheroid, $H_{\xi}^{\text{pr}}(\eta, \xi_0, \phi)$, can be written as

$$H_{\xi}^{\text{pr}}(\eta, \xi_0, \phi) = -\frac{H_0 d}{2} \sum_{m=0}^M \sum_{n=m}^N \sum_{p=0}^1 b_{\text{pmn}} P_n^m(\eta) P_n^m(\xi_0) T_{\text{pm}}(\phi), \quad (2)$$

where (η, ξ, ϕ) are the standard spheroidal coordinates; d is the spheroid's interfocal distance and P_n^m are associated Legendre functions of the first kind. By the orthogonality of the associated Legendre functions, the spheroidal expansion coefficients b_{pmn} can be derived as

$$b_{\text{pmn}} = -\frac{2n+1}{\gamma \pi H_0 d P_n^m(\xi_0)} \frac{(n-m)!}{(n+m)!} \int_{-1}^1 P_n^m(\eta) \int_0^{2\pi} H_{\xi}^{\text{pr}}(\eta, \xi_0, \phi) T_{\text{pm}}(\phi) d\phi d\eta, \quad (3)$$

where $\gamma = 2$ for $m = p = 0$ and $\gamma = 1$ otherwise. The integration in (3) is evaluated by numerical integration. This completes the decomposition of the primary field $H_{\xi}^{\text{pr}}(\eta, \xi_0, \phi)$.

After the primary magnetic field is decomposed into the pmn spheroidal modes, then the complete solution for the target to each $\mathbf{H}_{\text{pmn}}^{\text{pr}}$ field is obtained. Since the object is placed in a conducting and magnetically susceptible background, the magnetic field in the entire computational space (Regions 1 and 2, Figure 1) satisfies Helmholtz's wave equation and it can be represented with magnetic dipoles as

$$\mathbf{H}_\alpha(\mathbf{r}) = \int_S \bar{\bar{\mathbf{G}}}_\alpha(\mathbf{r}; \mathbf{r}') \cdot \mathbf{P}_\alpha(\mathbf{r}') ds' . \quad (4)$$

Here $\bar{\bar{\mathbf{G}}}_\alpha(\mathbf{r}; \mathbf{r}')$ is the Dyadic Green's Function, $\mathbf{P}_\alpha(\mathbf{r}')$ are amplitudes of magnetic dipoles, and $\alpha = 1, 2$ corresponds to region 1 or 2. Here

$$\bar{\bar{\mathbf{G}}}_\alpha(\mathbf{r}; \mathbf{r}') = \left(\bar{\bar{\mathbf{I}}} + \frac{\nabla \nabla}{k_\alpha^2} \right) \mathbf{G}_\alpha(\mathbf{r}; \mathbf{r}'), \quad \mathbf{G}_\alpha(\mathbf{r}; \mathbf{r}') \equiv \frac{e^{-jk_\alpha R}}{4\pi\mu_\alpha R} \quad (5)$$

$$k_\alpha = \sqrt{\omega\mu_\alpha\mu_0(\omega\epsilon_0 + j\sigma_\alpha)}$$

where $\bar{\bar{\mathbf{I}}}$ is the unit dyad, k_α is the wave-number in α region, σ_α and μ_α are conductivity and permeability of α region respectively, and $R \equiv |\mathbf{r} - \mathbf{r}'|$ is the distance between source and observation points. We assume that the relative electric permittivities of both regions are 1; $\mathbf{G}_\alpha(\mathbf{r}; \mathbf{r}')$ is the fundamental solution for the wave equation of the Hertzian magnetic vector potential, whereas the $\exp\{j\omega t\}$ time convention has been implied and suppressed.

On the surface of the object, total magnetic fields satisfy the following boundary conditions:

$$[\hat{\mathbf{n}} \times (\mathbf{H}_1^{\text{sc}} + \mathbf{H}^{\text{pr}})] = [\hat{\mathbf{n}} \times \mathbf{H}_2] \quad (6)$$

$$\hat{\mathbf{n}} \cdot \mu_1 (\mathbf{H}_1^{\text{sc}} + \mathbf{H}^{\text{pr}}) = \hat{\mathbf{n}} \cdot \mu_2 \mathbf{H}_2 \quad (7)$$

where $\hat{\mathbf{n}}$ is a unit normal vector on the real surface, \mathbf{H}^{pr} is the primary magnetic field, \mathbf{H}_2 is the total magnetic field in region 2, and μ_α is α region's relative magnetic permeability.

To determine amplitudes of the magnetic dipoles we have to solve the entire boundary value EMI problem for each mode of the primary field just once and then store the amplitudes of the responding sources. To do so, one extends each mode to the physical surface within the enclosing spheroid and applies the 3-D MAS-TSA method [24–25]. Finally, the target's response for each primary magnetic field component $\mathbf{b}_{\text{pnm}} \mathbf{H}_{\text{pnm}}^{\text{pr}}$ is expressed similar to (4) as:

$$\mathbf{H}_{\text{pnm}}^{\text{sc}}(\mathbf{r}) = \mathbf{b}_{\text{pnm}} \sum_{k=1}^N \bar{\bar{\mathbf{G}}}_1(\mathbf{r}, \mathbf{r}'_k) \mathbf{P}_{1,k}^{\text{pnm}} \quad (8)$$

where $\mathbf{P}_{1,k}^{\text{pnm}}$ is the amplitude of the k^{th} auxiliary magnetic dipole, located at the target's domain [24–25], corresponding to the $\mathbf{H}_{\text{pnm}}^{\text{pr}}$ response, and N is the number of auxiliary magnetic sources. Using $\mathbf{P}_{1,k}^{\text{pnm}}$ for each fundamental mode, the total response at any point outside the scatterer can be represented as:

$$\mathbf{H}^{\text{sc}}(\mathbf{r}) = \sum_{m=0}^{\infty} \sum_{n=m}^{\infty} \sum_{p=0}^1 b_{pmn} \sum_{k=1}^N \bar{\mathbf{G}}_1(\mathbf{r}, \mathbf{r}'_k) \mathbf{P}_{1,k}^{\text{pmn}}. \quad (9)$$

Thus, after pre-computation of the $\mathbf{P}_{1,k}^{\text{pmn}}$ coefficients for any given object, the EMI scattering problem, for any particular 3-D configuration involving it, breaks down merely to determine the spheroidal modal expansion coefficients b_{pmn} .

In equation (9) a substantial number of responding sources $\mathbf{P}_{1,k}^{\text{pmn}}$ are required to represent the scattered magnetic field outside the object (including physical surface). Similar to (9) we can re-express that field quite accurately in terms of a reduced number of sources from the fictitious spheroid. The amplitudes of this reduced number of sources $[\mathbf{p}^{\text{pmn}}]$ for each input pmn spheroidal mode can be determined by solving a linear system of equations for the normal component of the scattered magnetic field as it is shown in [24–25], and finally the complete secondary magnetic field can be represented as

$$\mathbf{H}^{\text{sc}}(\mathbf{r}) = \sum_{m=0}^{\infty} \sum_{n=m}^{\infty} \sum_{p=0}^1 b_{pmn} \sum_{i=1}^{N_{\text{red}}} \bar{\mathbf{G}}_1(\mathbf{r}, \mathbf{r}'_i) \mathbf{p}_i^{\text{pmn}}. \quad (10)$$

Note that, while we may ultimately be able to express the scattered field using a small number of sources, this is a fundamentally different strategy from what has been applied heretofore in the simple independent dipole models. In the latter, each source responds only to the primary field striking it locally. However, here the $\mathbf{p}_i^{\text{pmn}}, i = 1, 2, \dots, N_{\text{red}}$ responding sources act together, not in response to local stimuli but to express the response of the entire object to the distributed excitation of the pmn mode. In addition, using the MAS-MAS/TSA numerical code the $\mathbf{p}_i^{\text{pmn}}$ can be generated and stored for any number of pmn spheroidal modes in the infinite series (10). Once this is done, then the truncation criterion can be determined from the input primary magnetic field easily.

Overall, the entire SEA approach can be described briefly as follows:

1. For a given UXO amplitudes of responding magnetic dipoles $\mathbf{p}_i^{\text{pmn}}, i = 1, 2, \dots, N_{\text{red}}$ rings are determined and sorted in the universal library for any number of basic spheroidal mode excitations $pmn = 1, 2, \dots$
2. Once step 1 is done, then for a given sensor the primary field is decomposed into spheroidal modes, the spheroidal modal decomposition b_{pmn} coefficients are calculated, and the necessary number of spheroidal modes is determined.
3. Use reduced set of sources (RSS) $\mathbf{p}_i^{\text{pmn}}$ to calculate EMI response for each pmn -th basic excitation. Scale each pmn -EMI response on the b_{pmn} coefficients and calculate the target's complete response by just superposing responses of each basic excitation.

The GSEA, which is based on the MAS-TSA and introduced here, can produce a target's ultra-wideband frequency response. Thus, the proposed GSEA can be used directly to obtain an object's TD EMI responses via convolution theorem without recalculating amplitudes of the responding sources. This makes the GSEA a unified model to treat both FD and TD data, and is attractive from a practical point of view, thus many state-of-the-art EMI sensors (EM-63, EM-61, Zonge NanoTEM) are operating in TD.

Let us briefly describe the important formulas required to compute the TD EMI response for a general current waveform $I(t)$ flowing in a transmitter loop. By using the convolution theorem [29] the induced voltage in the receiver coil can be expressed as

$$\frac{dB}{dt} = -\int_0^t A'(t-\tau)I'(\tau)d\tau - A(0)I'(t) - A'(t)I(0), \quad (11)$$

where $A(t)$ represents an object's impulse response and the prime means the derivative with respect to time t . Equation (11) represents the TD response of an object to a general excitation current $I(t)$ source.

3. FREQUENCY-DEPENDENT MAGNETIC SUSCEPTIBILITY

There are three types of magnetic susceptibility that generate soils' EM responses: (1) induced, (2) permanent/remanent, and (3) viscous remanent (VRM). The soil magnetic properties are determined by the presence of iron and iron-oxide particles. Permanent remanent magnetization is the magnetization that exists in the absence of any applied field. Induced magnetization is the magnetization that arises in the presence of an external magnetic field, and viscous remanent magnetization (VRM) is a phenomenon that occurs when magnetization of an object placed in an external magnetic field changes in a time relative to the applied field. This means that the object's susceptibility is a complex frequency-dependent [9 and references therein]

$$\chi(\omega) = \chi'(\omega) + j\chi''(\omega) \quad (12)$$

where ω is the angular frequency, j is the unit complex number, and $\chi'(\omega)$ and $\chi''(\omega)$ are the real and imaginary parts for the frequency-dependent magnetic susceptibility. There are various references [31 and references therein] that discuss many aspects of soil magnetic properties. The most common frequency-dependent complex magnetic susceptibility, assuming that magnetic relaxation time constants are uniformly distributed between times τ_1 and τ_2 , is modeled as follows [31]:

$$\chi(\omega) = \chi_0 \left(1 - \frac{1}{\ln(\tau_2 / \tau_1)} \cdot \ln \frac{j\omega\tau_2 + 1}{j\omega\tau_1 + 1} \right) \quad (13)$$

where χ_0 is the D.C. value of the susceptibility.

For magnetically susceptible ground in the present of a metallic object, the field that is measured by the sensors contains two parts and can be written as

$$\mathbf{H}^{\text{mes}}(\omega) = \mathbf{H}^{\text{gr}}(\omega) + \mathbf{H}^{\text{obj}}(\omega) \quad (14)$$

where $\mathbf{H}^{\text{gr}}(\omega)$ and $\mathbf{H}^{\text{obj}}(\omega)$ are respectively magnetic fields produced by the magnetically susceptible soil and the object. The magnetic field \mathbf{H}^{obj} contains all interactions between the object and the susceptible host medium. For determining contribution of each magnetic field $\mathbf{H}^{\text{gr}}(\omega)$ and $\mathbf{H}^{\text{obj}}(\omega)$ in the measured field, a full EMI problem must be solved. In this paper the soil is considered to be a uniform half-space, and interaction between the soil and the object is taken into account by using the image source method [31].

4. NUMERICAL RESULTS

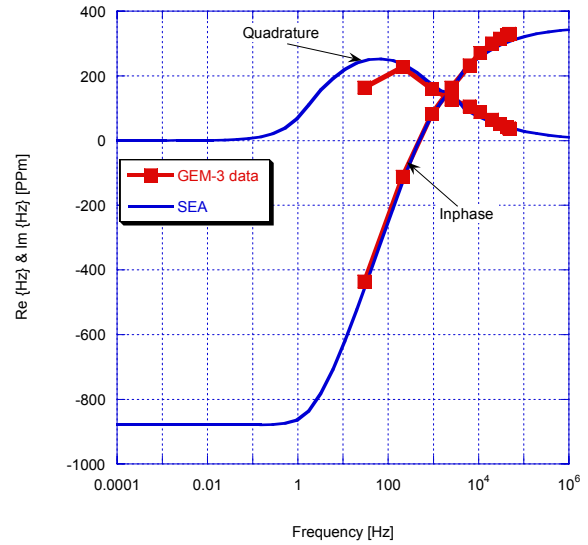
This section presents some numerical and experimental data that demonstrate the GSEA as a unified model for any FD or TD sensor configuration, and its applicability to complex data sets: novel waveforms, multi-axis, vector, or tensor magnetic, or electromagnetic induction data, or any combination of magnetic and EMI data; and ability to take into account the influence of conductive and magnetically susceptible geological soils on metal detectors.

a) *The universal RSS*

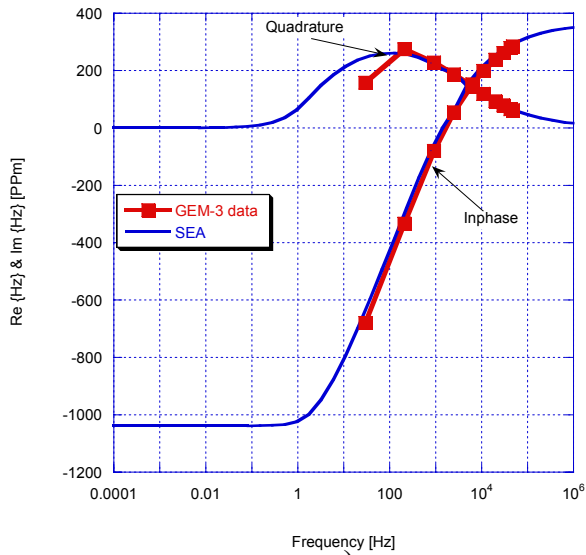
As it was discussed above, the reduced source set (RSS) $\mathbf{p}_i^{\text{pmn}}$ in Eq. (10) depends only on the target's geometry and electromagnetic properties. To validate such a unique characteristic of the RSS, here comparisons between RSS modeled and experimental data are given for an actual UXO (81 mm) in both FD and TD. The data were collected by two EMI systems that are widely used in the UXO discrimination community: (1) a wideband frequency-domain sensor



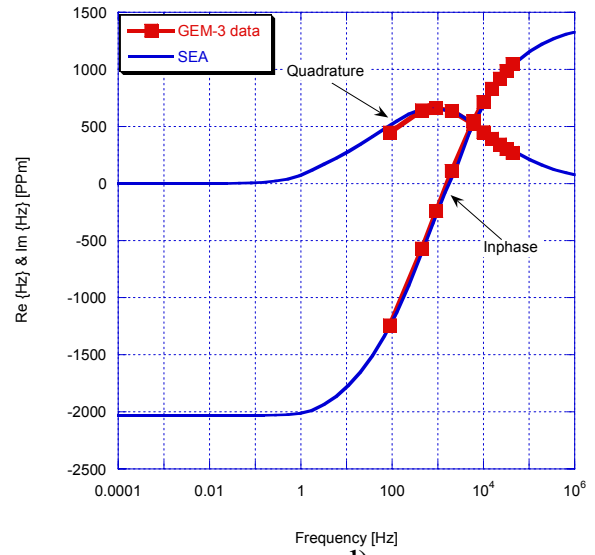
a)



b)



c)



d)

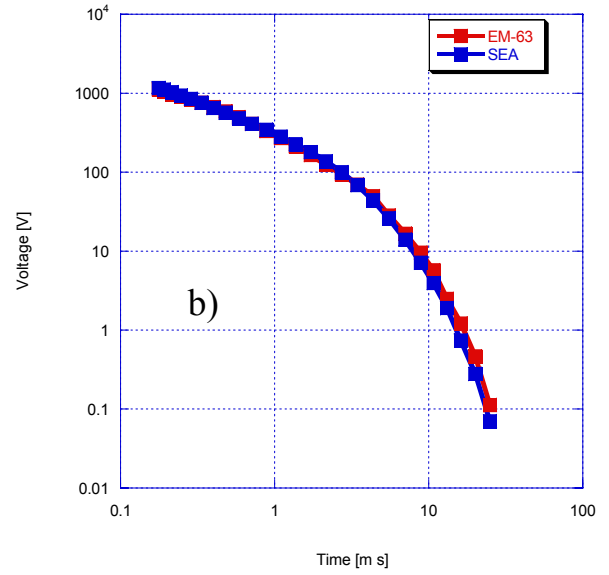
Figure 2. Frequency-domain EMI response for 81 mm UXO; (a) GEM-3 excitation; (b) nose up vertical, (c) nose up 45° inclination, (d) horizontal.

(GEM3) developed by Geophex Ltd. [2] and (2) a time-domain instrument (EM63) developed by Geonics [3]. The data were collected on the U.S. Army Engineer Research and Development Center test stand site.

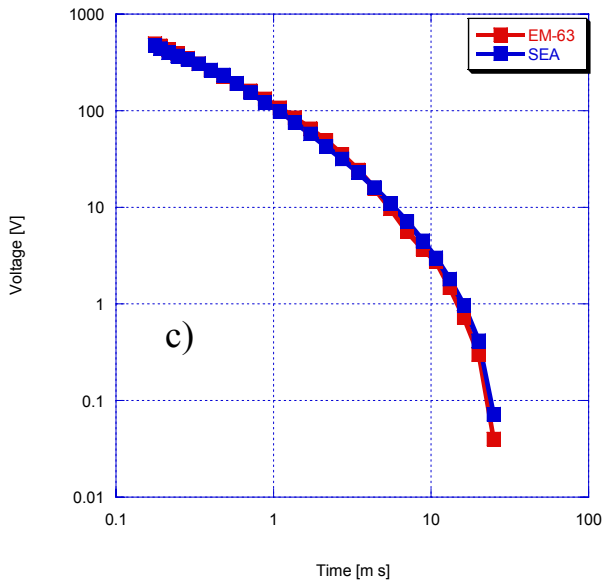
Figure 2 shows the comparisons between GSEA and actual data in the frequency domain. In this case data were collected for the UXO oriented in three different directions relative to the GEM-3 sensor's head: (1) vertical tail up, (2) 45° degree nose up, and (3) transverse. The GEM-3 frequency range is from 30 Hz to 50 kHz. The comparisons between measured and actual experimental data are in very good agreement for all orientations. Note that the RSS produces



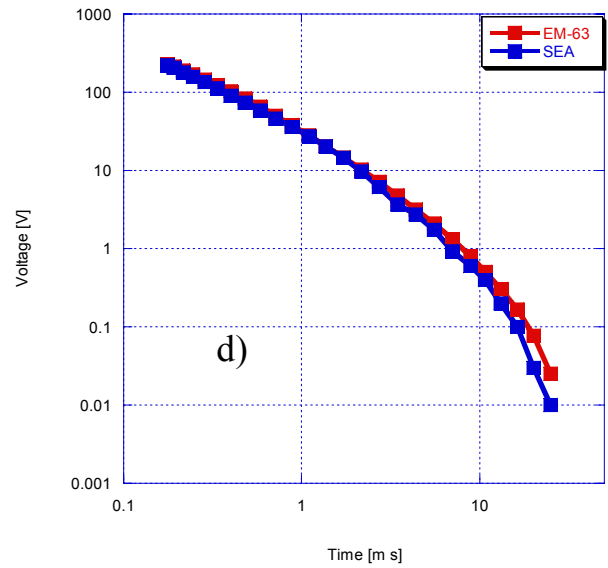
a)



b)



c)



d)

Figure 3. Time-domain EMI response for 81-mm UXO; (a) EM-3 excitation; (b) nose up vertical, (c) nose up 45° inclination, (d) horizontal.

results in an ultra-wideband frequency range, from magneto-static (0 Hz) to EMI frequency limit. This allows users to accurately compute the scattered field at any required frequencies by simple interpolation and to obtain EMI responses readily in TD via inverse Fourier transforms. To illustrate this capability, here the first impulse responses in TD are evaluated by applying the digital filter technique [28] to the inverse sine transform [29] as follows:

$$A(t) = \frac{2}{\pi} \int_0^{\infty} \text{Im } B(\omega) \sin \omega t \, d\omega, \quad (15)$$

where $\text{Im} B(\omega)$ represents an imaginary part of the magnetic flux that is calculated via RSS. Then the induced voltage is calculated using the time convolution technique (11).

In the EM63 instrument, the current waveform consists of an exponential current increase followed by a linear ramp off. The current has the three pulses per measurement. For comparisons between RSS and TD data, here the same 81-mm UXO is chosen. The object was excited from three: (1) vertical tail up, (2) 45° degree nose up, and (3) transverse orientations. For all three excitations, the vertical distance between the sensor's transmitter loop and the center of the cylinder is $h = 60.00$ cm. The TD induced voltage is calculated by an inverse Fourier transform of the frequency-domain magnetic field flux using equations (11) and (15). The comparisons are depicted in Figure 3. They show very good convergence between the measured and modeled TD data. Therefore, the universal RSS accurately produces EMI responses for a given target for any sensor in FD and TD domains.

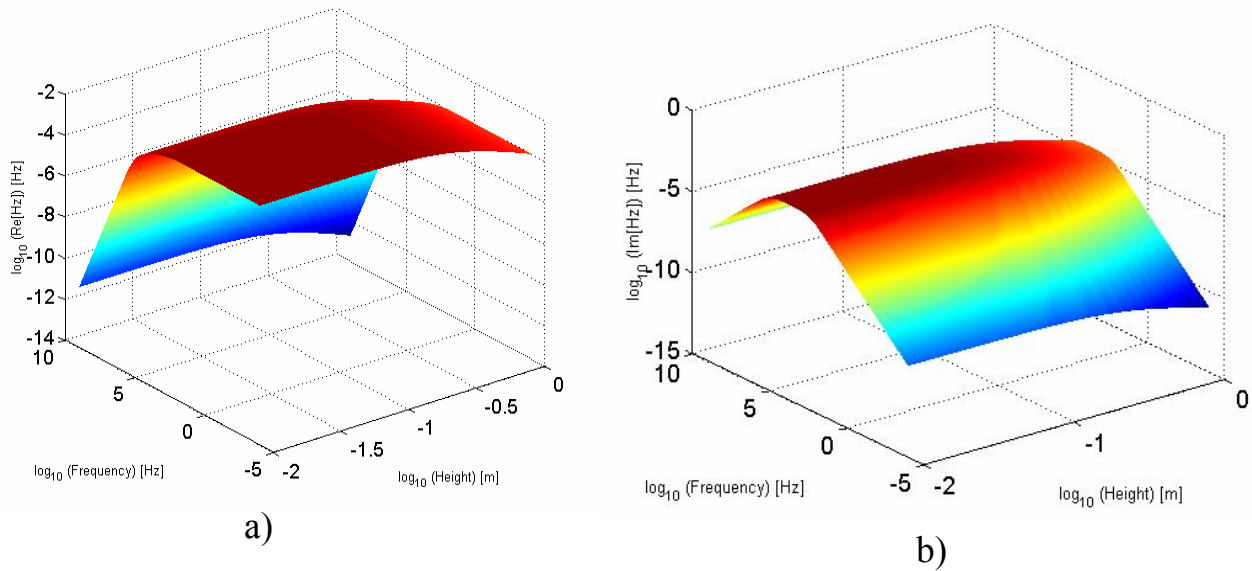


Figure 4. EMI response for a magnetically susceptible soil versus the sensor height and frequency.
(a) Inphase part; (b) quadrature part.

b) EMI response for soil with frequency-dependent susceptibility

In this section, first FD EMI response is studied for a magnetically susceptible half-space. The half-space is illuminated by a FD sensor. In these simulations for the sensor model the following parameters are used: current $I_0=1$ A, and a 100-cm \times 100-cm transmitter loop. The soil's frequency-dependent susceptibility is assumed to be the same as in equation (13) with a realistic $\chi_0 = 0.005$ D.C value of susceptibility [33], and $\tau_1 = 10^{-6}$ [sec] and $\tau_2 = 10^{-3}$ [sec] time constants. Figure 4 shows soil's responses in-phase (right) and quadrature (left) parts as a function of frequency and sensor height. The results illustrate that the soil's EMI responses strongly depend on both the frequency and sensor height. As the sensor approaches the soil, soil's response increases and it stays almost constant for antenna heights between 1 cm and 10 cm. Note that all parameters in Figure 4 are in Logarithmical scale. The soil response's quadrature part approaches to maximum between 10 kHz and 100 kHz, whereas at low frequencies the in-phase part is dominant. At highest frequencies (more than 100kHz) both parts of soil's response decrease. Thus a frequency-dependent magnetically susceptible soil produces significant EMI responses over entire UWB frequency range.

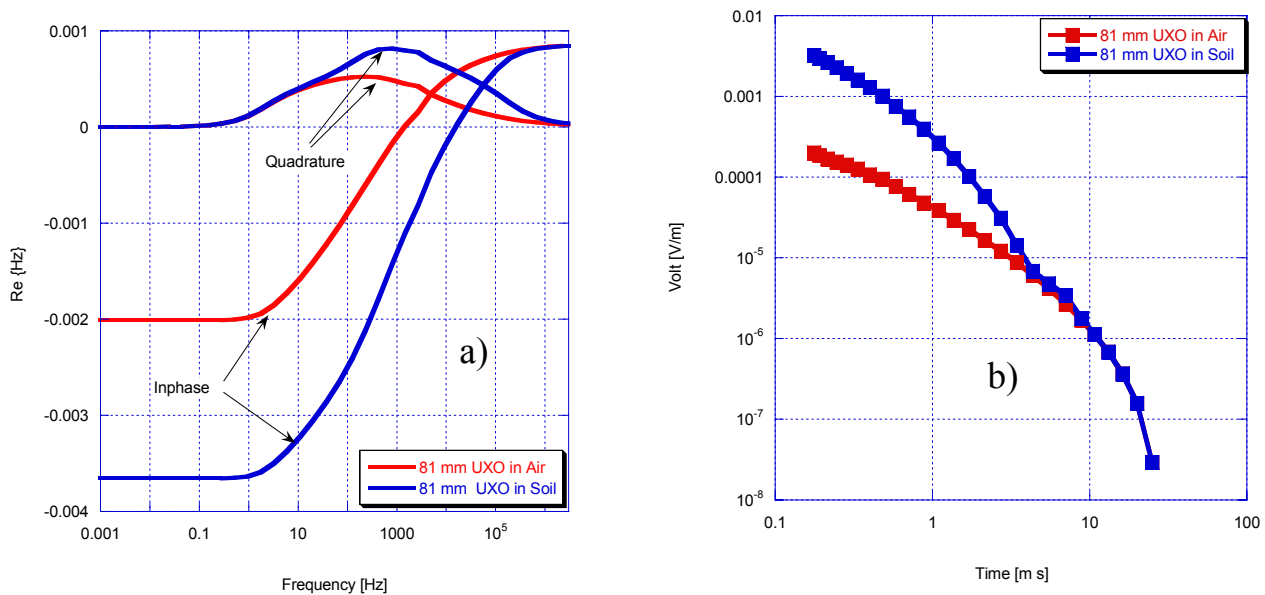


Figure 5. EMI response for 81 mm UXO; (a) Frequency domain, (b) Time domain.

Finally, to illustrate the soil effect on a buried object's EMI responses, several numerical experiments were done in both FD and TD. The 81-mm UXO was buried under a magnetically susceptible half-space. The half-space electromagnetic parameters are exactly the same ($\chi_0 = 0.005$, $\tau_1 = 10^{-6}$ [sec] and $\tau_2 = 10^{-3}$ [sec]) as in the previous paragraph. The entire structure is illuminated by (1) the GEM-3 sensor with current $I_o=1$ A, 10- and 20-cm radii coils, and (2) the EM-63 with $I_o=1$ A, 100-cm \times 100-cm transmitter loop. The sensors are placed 10 cm above the half-space. The UXO is oriented 45° nose up and its center is at 32-cm depth for the GEM-3 excitation and 50 cm for the EM-63 sensor. The results are depicted in Figure 5. These results clearly demonstrate that the magnetically susceptible half-space significantly affects both frequency and time domain EMI responses. In FD the magnetic soil modifies both in-phase and quadrature parts of the UXO response. Similarly, in TD the soil modifies the object's EMI response, and it appears at a very early time.

4. CONCLUSION

In this paper, the generalized standardized excitation approach, which is a fast, universal, and rigorous forward modeling system, has been developed and demonstrated. The GSEA is applicable to any FD or TD sensor configuration, and to any data set: novel waveforms, multi-axis, vector and tensor, or magnetic or electromagnetic induction data, or any combination of magnetic and EMI data.

The proposed system has been tested against actual data in both the frequency (GEM-3) and time (EM-63) domains. Excellent agreements between the GSEA and experimental data have been demonstrated here. The GSEA technique could be used for building a new type of EMI sensor as well as for optimal survey designing.

By using an appropriate dyadic Green's function the GSEA takes into account a host medium. EMI response from a magnetically susceptible half-space is analyzed versus sensor height and frequency. Numerical tests show that a frequency-dependent, magnetically susceptible half-space significantly affects the 81-mm UXO's EMI responses in both FD and TD. This study suggests that a magnetically susceptible host medium must be taken into account in UXO discrimination problems.

Acknowledgments

This work was supported by the Strategic Environmental Research and Development Program grant # SEED MM-1446.

References:

1. Billings, S.D. (2004) Discrimination and classification of buried unexploded ordnance using magnetometry. *IEEE Transactions of Geoscience and Remote Sensing*, 42, 1241–1251.
2. Won, I.J., D.A. Keiswetter; and T.H. Bell (2001) Electromagnetic induction spectroscopy for clearing landmines. *IEEE Trans. Geoscience and Remote Sensing*, Vol. 39, No. 4, pp. 703–709, April.
3. McNeill, J.D., and M. Bosnar (1996) Application of Time Domain Electromagnetic Techniques to UXO Detection. Proceedings of UXO Forum '96.
4. Cargile, D.M., H.H. Bennett, R.A. Goodson, T.A. DeMoss, and E.R. Cespedes (2004) Advanced UXO detection/discrimination technology demonstration, Kahoolawe, Hawaii. Technical Report ERDC/EL TR-04-1, U.S. Army Engineer Research and Development Center. Department of Defense, 2003. ESTCP cost and performance report (UX-0035): Geonics EM63 multichannel EM data processing algorithms for target location and ordnance discrimination. Technical Report UX-0035, Environmental Security Technology Certification Program.
5. Pasion, L.R., S.D. Billings, and D. Oldenburg (2002) Evaluating the Effects of Magnetic Susceptibility in UXO Discrimination Problems. SAGEEP Conference, Las Vegas, February 10–14, 2002.
6. Li, Y., and L.R. Pasion (2002) Evaluating the Effects of Magnetic Susceptibility in UXO Discrimination Problems Poster Presented at Partners in Environmental Technology Technical Symposium and Workshop. sponsored by SERDP and ESTCP, Washington, D.C., U.S.A., Dec 2002.
7. Pasion, L., S. Walker, D. Oldenburg, S. Billings, and J. Foley. (2005) Evaluating the Effectiveness of Varying Transmitter Waveforms for UXO Detection in Magnetic Soil Environments. Symposium on the Application of Geophysics to Engineering and Environmental Problems, Atlanta, Georgia, April 3–7, 2005.
8. Walker, S., L. Pasion, S. Billings, Y. Li, J. Foley, and D. Oldenburg (2005) Examples of the Effect of Magnetic Soil Environments on Time Domain Electromagnetic Data. Symposium on the Application of Geophysics to Engineering and Environmental Problems, Atlanta, Georgia, April 3–7, 2005.
9. Billings, S., L. Pasion, D. Oldenburg, and J. Foley (2003) The influence of magnetic viscosity on electromagnetic sensors. Proceedings of EUDEM-SCOT2, International Conference on Requirements and Technologies for the Detection, Removal and Neutralization of Landmines and UXO.
10. Shamatava, I., K. O'Neil, F. Shubitidze, K. Sun, and K.D. Paulsen (2005) Alter the EMI-BOR program to treat a permeable non-conducting medium. Proceedings of SPIE-2005.
11. Shubitidze, F., K. O'Neill, I. Shamatava, K. Sun, and K.D. Paulsen (2005) "Analyzing multi-axis data versus scalar data for UXO discrimination. Proceedings of SPIE-2005.
12. Sun, K., K. O'Neill, K., I. Shamatava, and K.d. Paulsen (2005) Discrimination of UXO buried under magnetic soil. Proceedings of SPIE-2005.
13. O'Neill, K., F. Shubitidze, K. Sun, I. Shamatava, and K.D. Paulsen (2005) EMI Obscuration of Buried UXO by Geophysical Magnetic Permeability, Anthropogenic Clutter, and by Magnitude Disparities. Proceedings of SPIE-2005.
14. Ware, G. (2003) Geonics EM63 multichannel EM data processing algorithms for target location and ordnance discrimination. Technical report, Environmental Security Technology Certification Program, UX-0035.
15. Bosnar, M. (2001) Discrimination of metallic targets in magnetically susceptible soil. U.S. Patent 6,326,791.
16. Remke L. van Dam, et al. (2005) Variability of magnetic soil properties in Hawaii. Proceedings of SPIE-2005, Orlando, Florida.
17. Geng, n., K.E. Baum, and L. Carin (1999) On the low frequency natural responses of conducting and permeable target. *IEEE Trans. Geoscience and Remote Sensing*, Vol. 37, pp. 347–359.
18. Gao, P., L. Collins, P. Garber, N. Geng, and L. Carin (2000) Classification of landmine-like metal targets using wideband electromagnetic induction. *IEEE Trans. Geoscience and Remote Sensing*, Vol. 38. No. 3., pp. 1352–1361.
19. Bell, T.H., B.J. Barrow, and J.T. Miller (2001) Subsurface discrimination using electromagnetic induction sensors. *IEEE Transactions on Geoscience and Remote Sensing*, volume: 39, issue 6, pp. 1286–1293, June.
20. Carin, L., Yu Haitao, Y. Dalichaouch, A.R. Perry, P.V. Czipott, and C.E. Baum (2001) On the wideband EMI response of a rotationally symmetric permeable and conducting target. *IEEE Trans. Geoscience and Remote Sensing*, Vol. 39, No. 6, pp. 1206–1213.
21. Miller, J.T. T. Bell, J. Soukup, and D. Keiswetter (2001) Simple phenomenological models for wideband frequency-domain electromagnetic induction. *IEEE Trans. Geoscience and Remote Sensing*, Vol. 39. No. 6., pp. 1294–1298, June.

22. Zhang, Y., L. Collins, H. Yu, C. Baum, and L. Carin (2003) Sensing of unexploded ordnance with magnetometer and induction: theory and signal processing. *IEEE Trans. Geoscience and Remote Sensing*, Vol. 41, No. 5, pp. 1005–1015, May.
23. Passion, L., and D.W Oldenburg (2001) A discrimination algorithm for UXO using time domain electromagnetics. *J. Eng. Environ. Geophys.*, vol. 28, pp. 91–102.
24. Shubitidze, F., K. O’Neill, I. Shamatava, K. Sun, and K.D. Paulsen (2005) Fast and accurate calculation of physically complete EMI response by a heterogeneous metallic object. *IEEE Transactions on Geoscience and Remote Sensing*, Volume 43, Issue 8, pp. 1736–1750.
25. Shubitidze, F., K., O’Neill, I. Shamatava, K. Sun, and K.D. Paulsen (2003) Analysis of EMI scattering to support UXO discrimination: Heterogeneous and multi objects. In *Proc. of SPIE “Detection and Remediation Technologies for Mines and Mine Like Targets,”* Orlando, Florida USA, pp. 928–939, April 21–25, 2003.
26. Sun, K., K. O’Neill, F. Shubitidze, I. Shamatava, and K.D. Paulsen (2005) Fast data-derived fundamental spheroidal excitation models with application to UXO discrimination. *IEEE Trans. Geosci. & Remote Sensing*, vol. 43, Issue 11, pp. 2573–2583.
27. McDonald, J.R. Technology needs for underwater UXO search and discrimination, SERP research project.
28. Andreasen, M.A. (1965) Scattering from bodies of revolution. *IEEE Trans. Antennas Propagat.* 13, pp. 303–310.
29. Anderson, W.L. (1982) Fast Hankel transforms using related and lagged convolutions. *ACM Transactions on Mathematical Software*, 8, 344–368.
30. Newman, G.A., G.W. Hohmann, and W.L. Anderson (1986) Transient electromagnetic response of a three-dimensional body in a layered earth. *Geophysics*, 51(8), 1608–1627.
31. Das, Y. (2004) A preliminary investigation of the effects of soils electromagnetic properties on metal detectors. Proceedings of SPIE, Volume 5415: Detection and Remediation Technologies for Mines and Minelike Targets IX, Russell S. Harmon, J. Thomas Broach, John H. Holloway, Jr., Editors, September 2004, pp. 677–690.
32. Jackson, J.D.(1998) *Classical electrodynamics: Third edition*. New York: John Wiley and Sons, Inc.
33. Walden, J., F. Oldfield, and J. Smith (2004) Environmental magnetism: A practical guide. *Quality Research Associate*.